The Astrophysical Journal Letters, 750:L29 (5pp), 2012 May 10 doi:10.1088/2041-8205/750/2/L29

MAGNETIC FIELD IN THE ISOLATED MASSIVE DENSE CLUMP IRAS 20126+4104

Hiroko Shinnaga[1], Giles Novak[2], John E. Vaillancourt[3], Masahiro N. Machida[4], Akimasa Kataoka[5], Kohji Tomisaka[6], Jacqueline Davidson[7], Thomas G. Phillips[1,8], C. Darren Dowell[9], Lerothodi Leeuw[10,11], and Martin Houde[7,12]

[1] California Institute of Technology Submillimeter Observatory, 111 Nowelo Street, Hilo, HI 96720, USA
[2] Department of Physics and Astronomy, Northwestern University, 633 Clark Street Evanston, IL 60208, USA
[3] Stratospheric Observatory for Infrared Astronomy, Universities Space Research Association, NASA Ames Research Center, Moffet Field, CA 94035, USA
[4] Department of Earth and Planetary Sciences, Faculty of Sciences, Kyushu University, 6-10-1 Hakozaki, Higashi-ku, Fukuoka 812-8581, Japan
[5] Department of Astronomy, Kyoto University, Kitashirakawa-Oiwake-cho, Sakyo-ku, Kyoto 606-8502, Japan
[6] National Astronomical Observatory of Japan and Department of Astronomy, School of Physical Sciences, Graduate University for Advanced Studies (SOKENDAI), Osawa 2-21-1, Mitaka, Tokyo 181-8588, Japan
[7] School of Physics, University of Western Australia, 35 Stirling Highway, Crawley WA 6009, Perth, Australia
[8] Division of Physics, Mathematics and Astronomy, California Institute of Technology, MC 320-47, Pasadena, CA 91125, USA
[9] Jet Propulsion Laboratory, California Institute of Technology, MS 169-506, 4800 Oak Grove Drive, Pasadena, CA 91109, USA
[10] SETI Institute, 515 North Whisman Avenue, Mountain View, CA 94043, USA
[11] Physics Department, University of Johannesburg, P.O. Box 524, Auckland Park 2006, South Africa
[12] Department of Physics and Astronomy University of Western Ontario, 1151 Richmond Street, London, Ontario N6A 3K7, Canada
Received 2011 December 2; accepted 2012 March 12; published 2012 April 18

ABSTRACT

We measured polarized dust emission at 350 μm toward the high-mass star-forming massive dense clump IRAS 20126+4104 using the SHARC II Polarimeter, SHARP, at the Caltech Submillimeter Observatory. Most of the observed magnetic field vectors agree well with magnetic field vectors obtained from a numerical simulation for the case when the global magnetic field lines are inclined with respect to the rotation axis of the dense clump. The results of the numerical simulation show that rotation plays an important role on the evolution of the massive dense clump and its magnetic field. The direction of the cold CO 1–0 bipolar outflow is parallel to the observed magnetic field within the dense clump as well as the global magnetic field, as inferred from optical polarimetry data, indicating that the magnetic field also plays a critical role in an early stage of massive star formation. The large-scale Keplerian disk of the massive (proto)star rotates in an almost opposite sense to the clump's envelope. The observed magnetic field morphology and the counterrotating feature of the massive dense clump system provide hints to constrain the role of magnetic fields in the process of high-mass star formation.

Key words: ISM: clouds – ISM: magnetic fields – polarization – stars: formation – submillimeter: ISM – techniques: polarimetric

1. INTRODUCTION

Massive stars deposit energy into the interstellar medium, and hence they may play a key role in regulating star formation in galaxies. Nevertheless, massive star formation is still poorly understood.

There are many difficulties in studying the formation of massive stars. Massive stars are rare and evolve quickly. The youngest phases of massive stars are poorly understood because they are deeply embedded in dense clumps. Often times massive stars form in cluster regions, which makes it difficult to disentangle the activities of each young massive star.

The early B type massive (proto)star, IRAS 20126+4104 ($\sim$7 $M_{\odot}$), is a well-studied unique target that allows us to observe the early stages of massive star formation in a simple configuration. The natal massive dense clump, which is a site of massive star formation, is an isolated rotating (2 km s^{-1} pc^{-1}) clump (Shinnaga et al. 2008) with a mass of $\sim$200 $M_{\odot}$ and temperature of 40 K (Shepherd et al. 2000). It has a large-scale bipolar outflow with a size scale of 0.5 pc (Shepherd et al. 2000; Shinnaga et al. 2008). The direction of this flow is very different from the direction of the smaller scale jet emanating from the massive (proto)star (Cesaroni et al. 1999), indicating that the jet might be precessing. The radial column density profile of the massive dense clump shows a shallow slope ($r^{-0.2}$) in an inner region within a radius of $\sim$0.13 pc, while the outer region of radius $\gtrsim$0.13 pc has a steeper slope ($\sim r^{-1.3}$), indicating that the inner region may be experiencing infall, while the infalling wave has not yet reached the outer region (Shinnaga et al. 2008). Another interesting feature of the massive dense clump is that the Keplerian disk, known to be associated with the (proto)star (Cesaroni et al. 1999, 2005), rotates almost in an opposite sense with respect to the rotation of the massive dense clump (Shinnaga et al. 2008).

Magnetic fields may play critical roles in star formation (McKee & Ostriker 2007). Here we report a study of the magnetic field of the massive dense clump, IRAS 20126+4104.

2. OBSERVATIONS AND DATA REDUCTION

We used the SHARC II Polarimeter, SHARP (Li et al. 2008), with the 10.4 m Leighton telescope at the Caltech Submillimeter Observatory (CSO) to measure dust polarization in the massive dense clump at 350 μm during 2007 August. SHARP uses the detector in SHARC II (Dowell et al. 2003) which has 384 pixels. Using the optics of SHARP, one divides the detector array into two sections, referred to as the H and V subarrays, for two orthogonal polarization components. Both polarization components are thus observed simultaneously. Each H and V subarray has 12 × 12 pixels with a field of view of $\sim 1' \times 1'$. The beam size was measured to be 9″. The data were acquired under good weather conditions. The 225 GHz opacity was measured

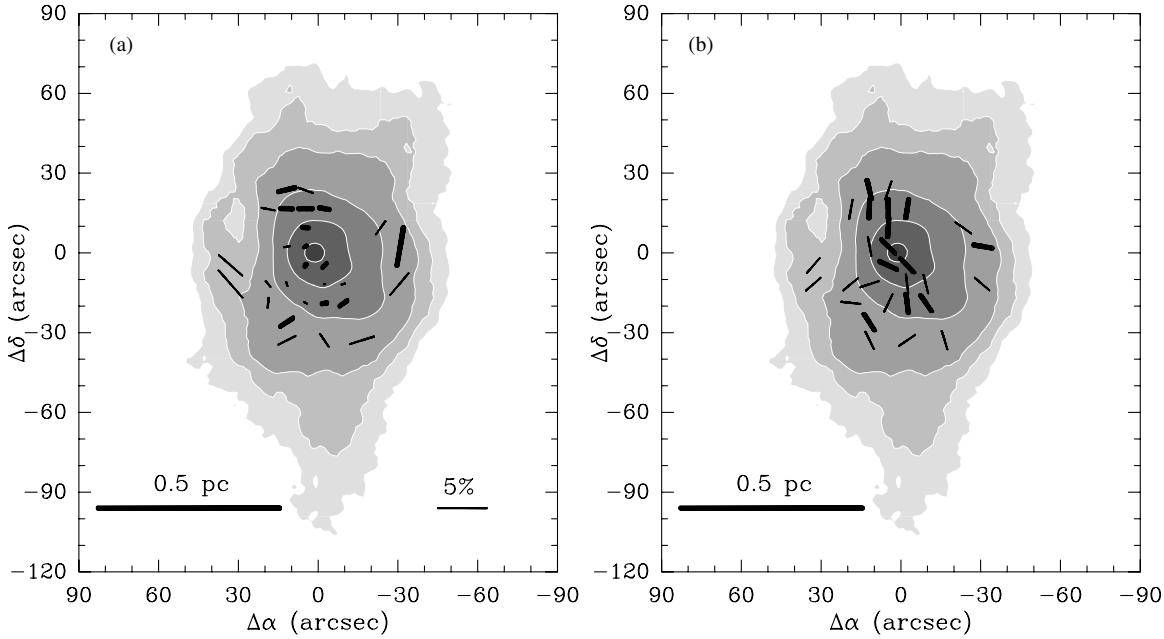

Figure 1. Black bars overlaid on the 350 μm dust continuum emission (gray scale) represent (a) the measured polarization E vectors at 350 μm and (b) the measured magnetic field directions. The length of the black bars in (a) is set to be proportional to the polarization degree. The length corresponding to 5% polarization degree is shown at bottom right of the diagram. The contours represent the 350 μm image obtained with SHARC II (Shinnaga et al. 2008) and are drawn at 2σ, 5σ, 9σ, 27σ, 81σ, and 243σ, where 2σ corresponds to 200 mJy beam^{-1}. Thick bars and thin bars are vectors with signal-to-noise ratio between 2.5σ and 6σ and between 2σ and 2.5σ, respectively.

to be from 0.04 to 0.07. Using the peak of the dust continuum emission, pointing corrections were made. Pointing errors were estimated to be under $\sim 2''$. A reduced-χ^2 analysis of Q and U data (Davidson et al. 2011) was performed to obtain the final polarization map. The reduced χ^2 was found to be 1.87 ± 1.21 when dividing the data into eight bins. The error bars for the polarization degree and magnetic field direction were inflated accordingly.

3. RESULTS AND DISCUSSION

3.1. Measured Polarization and Magnetic Field

Figure 1(a) shows the polarization vectors measured at 350 μm with SHARP. The degree of polarization in the envelope region is higher than that in the central region of the clump. Such a tendency, i.e., polarization hole, is observed toward other star-forming regions such as Orion (Schleuning 1998) and W3 (Schleuning et al. 2000). Schleuning (1998) argues that the decrease of polarization degree may be caused by temperature and/or optical depth effects. For the case of IRAS 20126+4104, the temperature structure appears to be complicated, as discussed in Shinnaga et al. (2008). The fact that vectors outside of the third contour from the peak of the dust continuum have larger polarization degrees compared to the vectors inside the third contour (Figure 1) suggests that the polarization hole may be caused by optical depth effects. Matthews et al. (2009) reported the dust polarization of this object at 850 μm. The polarization vectors measured with SHARP are located in the central $r \sim 0.3$ pc region of the massive dense clump, while the polarization vectors measured at 850 μm trace a region outside of $r \sim 0.2$ pc but within the $r \sim 0.5$ pc region. Overall, the polarization vectors of Matthews et al. (2009) agree well with our 350 μm polarization vectors.

The magnetic field directions are obtained by flipping the polarization vectors by 90° as plotted in Figure 1(b). Looking at the magnetic field directions along a north–south line passing through the center of the massive dense clump, one notices that many of these vectors (except for the central $\sim$0.1 pc region) roughly follow the north–south direction. On the other hand, for the east and west sides of the clump, many of the magnetic field directions tend to follow an east–west direction rather than a north–south direction. This tendency persists in the regions where 850 μm polarization vectors are observed. Detailed comparison between the 350 μm polarization vectors and the 850 μm polarization vectors will be described elsewhere. The magnetic field changes its direction inside the infalling region, i.e., for radii below 0.1 pc.

3.2. Comparison with Simulation Results

To investigate the morphological evolution of magnetic field lines, we calculated the evolution of a magnetized cloud using a three-dimensional resistive magnetohydrodynamics nested grid code with an isothermal equation of state and sink cell treatment (Machida et al. 2005; 2011a). Details are described in A. Kataoka et al. (in preparation). To conduct the simulation, we set the parameters so that they are close to the observed parameters of the massive dense clump IRAS 20126+4104.

The schematic diagram in Figure 2 shows the initial state, which is a spherical cloud core with a critical Bonnor–Ebert (BE) density profile. The BE profile is characterized by two parameters, the central number density (n_c) and the isothermal temperature (T_{iso}). We adopt $n_c = 6 \times 10^3$ cm^{-3} with the density enhancement factor of $f = 1.68$ (Machida et al. 2011b) and $T_{iso} = 40$ K. Then, a uniform magnetic field ($B = 1.5 \times 10^{-5}$ G) parallel to the z-axis is imposed on the whole computational domain. The reason why we set the magnetic field direction to be parallel to the z-axis is because the direction of the observed global magnetic field is almost north–south (see Section 3.4). In addition, rigid rotation ($\Omega_0 = 1.1 \times 10^{-14}$ s^{-1} = 0.35 km s^{-1} pc^{-1}) is added to the initial state, in which the

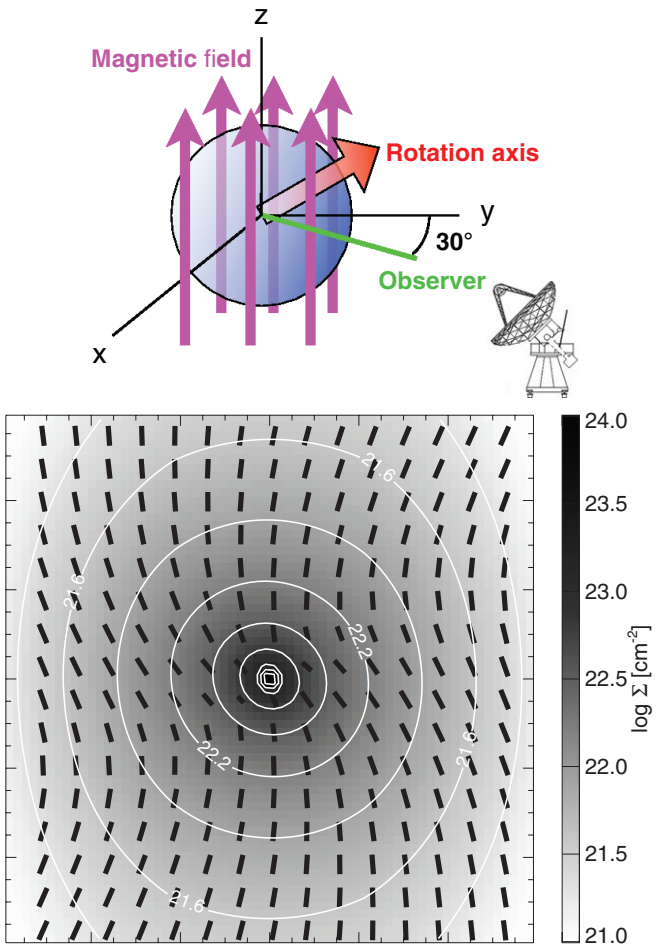

Figure 2. Top: the schematic diagram summarizes the initial state of the simulation. The blue sphere represents the spherical cloud core, being penetrated by magnetic field (purple vectors) along the z-axis. The rotation axis of the cloud core is inclined by 60° from the z-axis on the y–z plane, as shown by the big red arrow. Note that observers view the cloud core from a direction that is inclined by 30° from the y-axis on the x–y plane. Bottom: the diagram shows the resultant magnetic field vectors (black bars) and the column density (gray scale and white contours) calculated from the numerical simulation. White contours and gray scale represent the column density of the dense clump. The protostar has a mass of 7.3 $M_\odot$ and a large fraction of the cloud mass remains as the infalling envelope. The size of the diagram is 1.2 $\times 10^5$ by 1.2 $\times 10^5$ AU (=0.6 pc).

rotation axis, defined by right-hand rule, is inclined with respect to the magnetic field (i.e., z-axis) at an angle of 60° on the y–z plane, as shown in the schematic diagram of Figure 2. The observer views the simulation from a point in the x–y plane. This is shown in Figure 2, where it can be seen that the observer's line of sight is inclined by an angle of 30° with respect to the y-axis. On the plane of the sky, the rotation axis becomes P.A. $\sim -40°$, close to the P.A. $= -35°$ rotation axis of the large-scale Keplerian disk (radius of 7400 AU (0.037 pc); Cesaroni et al. 1999), which is situated at the center of the dense clump. With these assumptions, the initial cloud has a radius of 1.2×10^5 AU (= 0.6 pc) and mass of 78 $M_\odot$.

The initial cloud has the energy ratios of $E_{\rm thermal}/E_{\rm gravity} = 0.5$, $E_{\rm rotation}/E_{\rm gravity} = 0.02$, and $E_{\rm magnetic}/E_{\rm gravity} = 0.55$, where $E_{\rm thermal}$, $E_{\rm rotation}$, $E_{\rm magnetic}$, and $E_{\rm gravity}$ are thermal, magnetic, rotational, and gravitational energy, respectively. In the calculation, we assumed the protostar formation to occur when the central density exceeds the threshold number density $n_{\rm thr} = 10^8$ cm^{-3} in the region of radius less than accretion radius, $r_{\rm acc}$, where $r_{\rm acc} = 64$ AU is adopted as the sink radius (for details, see Machida et al. 2011a). With this treatment, we calculated the cloud evolution until the gas accretion onto the protostar or circumstellar disk almost halts. To directly compare simulation results with our observations, we calculated polarization of thermal dust emission using the formulation in Tomisaka (2011), in which we assume that the whole region is optically thin and isothermal for simplicity.

The bottom diagram of Figure 2 shows our simulation result, in which magnetic field vectors and column density 7.1 $\times 10^5$ yr after the cloud collapse begins (or 8 $\times 10^4$ yr after the protostar formation) are plotted. The 30° viewing angle (the top diagram of Figure 2) was chosen because it gives the best agreement between the observed and simulated magnetic field vectors. In particular, note that both Figures 1(b) and 2 show an S shape as one moves from north to south. At the epoch shown in the figure, the protostar has a mass of 7.3 $M_\odot$ and a large fraction of the cloud mass remains in the infalling envelope. Note that radiative heating from the central protostar is ignored.

In a real high-mass star-forming region, one can expect in general that the rotation axis of a dense clump will not be aligned with the magnetic field. In this situation, simulations sometimes show the magnetic field morphology in an hourglass shape, but not always. Also, the observed shape of the magnetic field changes depending on the observer's viewing angle. For the simulation shown in Figure 2, the observed magnetic field vectors are aligned nearly in an S shape, but the morphology of the magnetic field vectors takes an hourglass shape if one observes the magnetic field along the x-axis.

In order to reproduce the observed magnetic field morphology, the effect of the rotation of the dense clump was found to be essential. This may imply that the rather fast rotation of the massive dense clump may have determined the magnetic field directions within the central regions of the massive dense clump, as well as the axis of the jet/Keplerian disk system associated with the central massive (proto)star. In our simulation, we do see the expected toroidal field generated by the rotating disk at the cloud's center. We cannot resolve it in Figure 2 because the scale of the toroidal field ($\sim 10^3$ AU) is much smaller than the cloud scale ($\sim 10^5$ AU). Although the dominant components of the observed magnetic field presumably come from large-scale structure, the innermost vectors of our magnetic field map may show a hint of the toroidal disk field. Although the dominant components of the observed magnetic field come from large-scale structure, we might have detected a hint of toroidal field generated by the rotating disk.

The configuration of the magnetic field lines is related to the rotating disk that has a size of $\sim$1000 AU. Since the sink radius adopted in this study (64 AU) is much smaller than the rotating disk, we can spatially resolve it. However, the resultant disk size may be dependent on the sink radius because we cannot resolve the early phase of the disk evolution.

3.3. The Magnetic Field and Its Relationship with the Clump's Rotation, the Bipolar Outflow, and the Jet Directions

Based on the observed velocity gradient of the narrow line components, the rotation axis of the massive dense clump is roughly 140° $\pm$ 20° in P.A., where we again use the right-hand rule (Shinnaga et al. 2008). On the other hand, the edge-on Keplerian disk of the massive (proto)star appears to rotate in almost the opposite sense to the rotation of the envelope of the massive dense clump whose effective radius is 0.56 pc (=1.15 $\times$ 10^5 AU; Cesaroni et al. 2005; Shinnaga

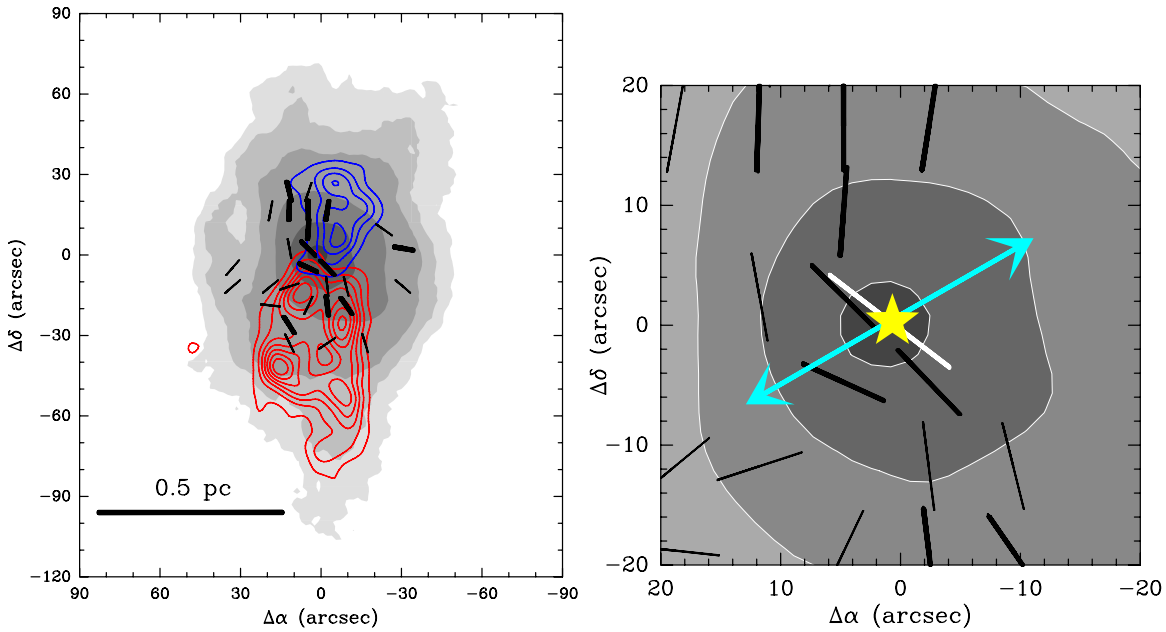

Figure 3. Left: molecular bipolar outflow lobes traced in the CO $J = 1$–0 line (same as Figure 13 of Shinnaga et al. 2008) overlaid on the diagram of Figure 1(b). Right: white line and light blue arrows represent the direction of the Keplerian disk (P.A. $\sim 53^\circ$) and the direction of the jet (P.A. $\sim -60^\circ$) associated with the massive (proto)star (Cesaroni et al. 1999), marked with a yellow star, overlaid on the diagram of Figure 1(b), magnified in the central region.

et al. 2008). Machida et al. (2006) discuss the cases when the rotation axis of a circumstellar disk is inclined with respect to the magnetic field axis. Under the conditions considered in their paper, i.e., a quiescent cloud core that forms low-mass stars, the counterrotation between cloud core and disk, as seen in IRAS 20126+4104, cannot occur. Mouschovias & Paleologou (1979) first discussed the counter-rotating feature through magnetic breaking (see also Nakano 1989). Machida et al. (2011b) discuss the importance of magnetic braking on the circumstellar disk formation in a strongly magnetized cloud. The kind of counterrotation observed in this object might happen when the angular momentum of a circumstellar disk is extremely efficiently transferred through magnetic braking.

The two diagrams of Figure 3 show the cold bipolar outflow traced with CO $J = 1$–0 and the directions of the jet/Keplerian disk plane, overlaid on the magnetic field directions and the 350 μm dust continuum map (same as Figure 1(b)). The jet axis has P.A. $\sim -60^\circ$. Comparing the bipolar outflow axis with the directions of the magnetic field in the massive dense clump, they are nearly parallel. For the warm bipolar outflow traced with CO $J = 6$–5, the direction is very different (see Figure 12 of Shinnaga et al. 2008), particularly the blue lobe is in a northwest–southeast direction with a smaller size than that of CO 1–0. The direction of the CO 6–5 outflow is close to the direction of the jet emanating from the massive (proto)star. The observed magnetic field directions near the Kelperian disk appear to lie parallel to the disk plane, which means at this location the fields are nearly perpendicular to the jet axis.

Ciardi & Hennebelle (2010) report numerical simulations of outflows in collapsing dense cores with misaligned rotation and magnetic field axes and find that a larger angle α between the rotation axis and the magnetic field direction leads to decreased efficiency of mass ejection via outflows. The reason why the size of the CO $J = 1$–0 bipolar outflow in IRAS 20126+4104 is larger than that of the CO $J = 6$–5 outflow (Shinnaga et al. 2008) may be that α for the 1–0 outflow is smaller than that of the 6–5 outflow. Ciardi & Hennebelle (2010) also found that the misalignment of magnetic field and rotation axes leads to jet precession. The apparent precession of the jet associated with the massive (proto)star in IRAS 20126+4104 thus may be explained by the misalignment of magnetic field and rotation axis. An alternative explanation for precession is that the source at the clump center is binary, but observational studies carried out to date do not show evidence of binarity.

3.4. The Magnetic Field in the Massive Dense Clump and the Global Magnetic Field

It is of interest to compare the magnetic field direction in the massive dense clump and the global magnetic field surrounding the clump (e.g., Li et al. 2009). The global magnetic field direction around this object is estimated using the optical polarization data archive of Heiles (2000). The polarization data points that meet the following criteria were selected to trace the global magnetic field: (1) within $\pm$ 200 pc from the distance of the object (1500 pc) for the direction along the line of sight, and (2) within 2° (roughly 50 pc in radius) from the center of the massive dense clump on the plane of sky. The polarization data points and the mean direction of the global magnetic field are plotted in Figure 4. Note that four polarization data points that are within $\sim 0.^\circ 8$ of the center of the nearby supernova remnant (SNR) G78.2+2.1 are omitted in this diagram because their polarization vectors are likely to be affected by the SNR. The threshold of $0.^\circ 8$ was determined based on the radio continuum map of Wendker (1984). One sees that the global magnetic field is more or less aligned in a north–south direction, i.e., in the same direction as the CO 1–0 bipolar outflow. The massive dense clump is elongated in a north–south direction. The mean direction of the global magnetic field is P.A. $\sim -3^\circ$. The fact that the CO 1–0 bipolar outflow is parallel to the global magnetic field suggests that the magnetic field had a significant influence on the star formation process (Matsumoto & Tomisaka 2004). However, the deeply embedded Keplerian disk and the jet show no such alignment with the global magnetic field. They seem to be aligned with the rotation axis of the dense clump.

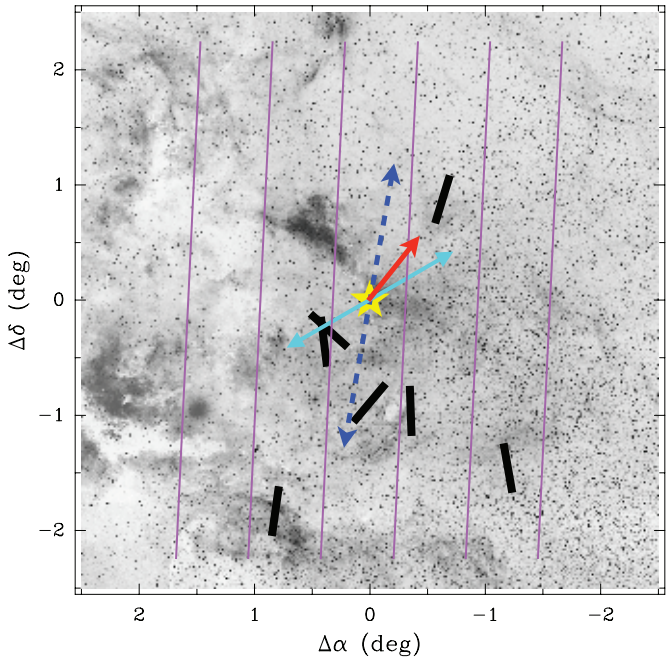

Figure 4. Optical polarization vectors (black thick lines) are superposed on an optical image (DSS 0.5 μm, gray scale) centered on IRAS 20126+4104. The yellow star marks the position of the massive (proto)star. Purple thin lines represent the mean direction of the global magnetic field (P.A. $\sim -3°$). Blue thick dashed arrows show the direction of the CO 1–0 bipolar outflow (P.A. $\sim -10°$). The red arrow and the light blue arrows represent the rotation axis of the large Keplerian disk (P.A. $\sim -37°$) and the directions of the jet (P.A. $\sim -60°$) associated with the massive (proto)star, respectively.

4. SUMMARY AND FUTURE WORK

In order to measure the magnetic field structure of the massive dense clump IRAS 20126+4104, polarized dust emission was measured at 350 μm. The observed magnetic field is consistent with the magnetic field vectors of a simulation when magnetic field lines are inclined from the rotation axis of the dense clump. As an evidence that the magnetic field played a critical role on the formation of the massive (proto)star, the magnetic field directions within the massive dense clump are parallel to the CO 1–0 bipolar outflow direction and appear to connect to the global magnetic field. Our observational data combined with the simulation results indicate that the rotation of the massive dense clump affects the magnetic field within the clump as well as the orientation of the Keplerian disk/jet system. The counterrotation feature observed between the envelope of the dense clump and the large rotating disk associated with the massive (proto) star might be a result of efficient angular momentum transfer via magnetic braking (e.g., Machida et al. 2011b). This issue should be further addressed in the future in order to fully understand the role of magnetic field in the star formation processes. It is important to measure the magnetic field strength within the massive dense clump using Zeeman effect in order to investigate the details of the evolution of the massive (proto)star and of the natal dense clump.

This research has been supported by the NSF grants AST-0540882 and AST-0838261 to the CSO. SHARP has been supported by the NSF grants AST 02-41356, AST 05-05230, and AST-0909030 to Northwestern University and grant AST 05-05124 to the University of Chicago. Numerical computations were carried out on NEC SX-9 and the general-purpose PC farm at Center for Computational Astrophysics of National Astronomical Observatory of Japan. This work was supported by a Grants-in-Aid from MEXT (21740136,21244021). Part of this work was carried out at the Jet Propulsion Laboratory, California Institute of Technology, under a contract with the National Aeronautics and Space Administration. H.S. thanks Hua-bai Li, Roger Hildebrand, and Fumitaka Nakamura for helpful comments, and Shu-ichiro Inutsuka for valuable discussions.

Facility: CSO

REFERENCES

Cesaroni, R., Felli, M., Jenness, T., et al. 1999, A&A, 345, 949
Cesaroni, R., Neri, R., Olmi, L., et al. 2005, A&A, 434, 1039
Ciardi, A., & Hennebelle, P. 2010, MNRAS, 409, L39
Davidson, J. A., Novak, G., Matthews, T. G., et al. 2011, ApJ, 732, 97
Dowell, C. D., Allen, C. A., Babu, R. S., et al. 2003, Proc. SPIE, 4855, 73
Heiles, C. 2000, AJ, 119, 923
Li, H., Dowell, C. D., Kirby, L., Novak, G., & Vaillancourt, J. E. 2008, Appl. Opt., 47, 422
Li, H.-b., Dowell, C. D., Goodman, A., Hildebrand, R., & Novak, G. 2009, ApJ, 704, 891
Machida, M. N., Inutsuka, S., & Matsumoto, T. 2011a, ApJ, 729, 42
Machida, M. N., Inutsuka, S., & Matsumoto, T. 2011b, PASJ, 63, 555
Machida, M. N., Matsumoto, T., Hanawa, T., & Tomisaka, K. 2005, MNRAS, 362, 382
Machida, M. N., Matsumoto, T., Hanawa, T., & Tomisaka, K. 2006, ApJ, 645, 1227
Matsumoto, T., & Tomisaka, K. 2004, ApJ, 616, 266
Matthews, B. C., McPhee, C. A., Fissel, L. M., & Curran, R. L. 2009, ApJS, 182, 143
McKee, C. F., & Ostriker, E. C. 2007, ARA&A, 45, 565
Mouschovias, T. C., & Paleologou, E. V. 1979, ApJ, 230, 204
Nakano, Y. 1989, MNRAS, 241, 495
Schleuning, D. A. 1998, ApJ, 493, 811
Schleuning, D. A., Vaillancourt, J. E., Hildebrand, R. H., et al. 2000, ApJ, 535, 913
Shepherd, D. S., Yu, K. C., Bally, J., & Testi, L. 2000, ApJ, 535, 833
Shinnaga, H., Phillips, T. G., Furuya, R. S., & Cesaroni, R. 2008, ApJ, 682, 1103
Tomisaka, K. 2011, PASJ, 63, 147
Wendker, H. J. 1984, A&AS, 58, 291